Versatile click alginate hydrogels with protease-sensitive domains as cell responsive/instructive 3D microenvironments

Carbohydrate Polymers 320 (2023) 121226

Contents lists available at ScienceDirect

Carbohydrate Polymers

journal homepage: www.elsevier.com/locate/carbpol

Versatile click alginate hydrogels with protease-sensitive domains as cell responsive/instructive 3D microenvironments

Mariana I. Neves [a,b,c,1], Mariana V. Magalhães [a,b,c,1], Sílvia J. Bidarra [a,b], Lorenzo Moroni [d,e], Cristina C. Barrias [a,b,f,*]

[a] i3S – Instituto de Investigação e Inovação em Saúde, Universidade do Porto, R. Alfredo Allen 208, 4200-135 Porto, Portugal
[b] INEB – Instituto de Engenharia Biomédica, Universidade do Porto, Portugal
[c] FEUP – Faculdade de Engenharia, Universidade do Porto, Portugal
[d] Department of Complex Tissue Regeneration, MERLN Institute for Technology-Inspired Regenerative Medicine, Maastricht University, Maastricht, Netherlands
[e] CNR NANOTEC - Institute of Nanotechnology, Università del Salento, Lecce, Italy
[f] ICBAS – Instituto de Ciências Biomédicas Abel Salazar, Universidade do Porto, Portugal

ARTICLE INFO

Keywords:
Matrix remodeling
Protease sensitive
Bioactive
Bio-orthogonal

ABSTRACT

Alginate (ALG) is a widely used biomaterial to create artificial extracellular matrices (ECM) for tissue engineering. Since it does not degrade in the human body, imparting proteolytic sensitivity to ALG hydrogels leverages their properties as ECM-mimics. Herein, we explored the strain-promoted azide-alkyne cycloaddition (SPAAC) as a biocompatible and bio-orthogonal click-chemistry to graft cyclooctyne-modified alginate (ALG-K) with bi-azide-functionalized PVGLIG peptides. These are sensitive to matrix metalloproteinase (MMP) and may act as crosslinkers. The ALG-K-PVGLIG conjugates (50, 125, and 250 μM PVGLIG) were characterized for peptide incorporation, crosslinking ability (double-end grafting), and enzymatic liability. For producing cell-permissive multifunctional 3D matrices for dermal fibroblast culture, oxidized ALG-K was grafted with PVGLIG and with RGD peptides for cell-adhesion. SPAAC reactions were performed immediately before cell-laden hydrogel formation by secondary ionic-crosslinking, considerably reducing the steps and time of preparation. Hydrogels with intermediate PVGLIG concentration (125 μM) presented slightly higher stiffness while promoting extensive cell spreading and higher degree of cell-cell interconnections, likely favored by cell-driven proteolytic remodeling of the network. The hydrogel-embedded cells were able to produce their own pericellular ECM, expressed MMP-2 and 14, and secreted PVGLIG-degrading enzymes. By recapitulating key ECM-like features, these hydrogels provide biologically relevant 3D matrices for soft tissue regeneration.

1. Introduction

Alginate hydrogels are among the most popular biomaterials for cell delivery and tissue engineering approaches, where they have been extensively used as artificial extracellular matrices (ECM) (Bidarra et al., 2014; Neves et al., 2020). These natural algae-derived polysaccharides present a linear backbone comprised of repeating (1,4)-linked β-D-mannuronic and α-Lguluronic acid motifs and can form hydrogels via a variety of ionic and covalent crosslinking methods (Cao et al., 2020). Ionic crosslinking in the presence of divalent cations presents unique advantages, being simple, mild, fast, and reversible (Cao et al., 2020). While alginate hydrogels afford cytocompatible 3D microenvironments with high hydration, permeability, and adequate mechanical properties, they are essentially bioinert. This can be regarded as an advantage for matrix engineering, as alginate hydrogels provide ideal blank-slates for customized biofunctionalization, namely with bioactive moieties (Fonseca et al., 2013; Maia, Fonseca, et al., 2014). For example, their covalent modification with integrin-binding RGD peptides is a widely used strategy and a mandatory requirement to promote cell-matrix adhesion (Bidarra et al., 2011; Rowley et al., 1999). In 3D culture, the polymeric network imposes a physical barrier to embedded cells, restricting motility, spreading, proliferation and endogenous ECM production

* Corresponding author at: i3S – Instituto de Investigação e Inovação em Saúde, Universidade do Porto, Portugal.
E-mail addresses: mariana.neves@i3s.up.pt (M.I. Neves), mariana.magalhaes@i3s.up.pt (M.V. Magalhães), sbidarra@ineb.up.pt (S.J. Bidarra), l.moroni@maastrichtuniversity.nl (L. Moroni), ccbarrias@i3s.up.pt (C.C. Barrias).
[1] Authors contributed equally to this work.

https://doi.org/10.1016/j.carbpol.2023.121226
Received 5 May 2023; Received in revised form 18 July 2023; Accepted 19 July 2023
Available online 22 July 2023

(Fonseca et al., 2011). Thus, the modification of alginate hydrogels with degradable motifs is often required to improve their properties as ECM-mimics. In native tissues, ECM remodeling is involved in several biological events, including tissue formation, repair, and regeneration (Xu et al., 2022; Xue & Jackson, 2015). To mimic this dynamic process and support neo-tissue formation in vitro, cell responsive hydrogels have been designed to allow proteolytic degradation (Fonseca, Granja, & Barrias, 2014; Lueckgen et al., 2020; Rowley et al., 2019). Matrix metalloproteinases (MMPs) are a family of endopeptidases that have the capacity to degrade almost every protein component of the ECM, playing a pivotal role in matrix remodeling and turnover processes (Loffek et al., 2011). For this reason, peptide sequences cleavable by MMPs, such as the proline-valine-glycine-leucine-isoleucine-glycine (PVGLIG) peptide sequence, have been previously incorporated in 3D hydrogel networks to render them susceptible to enzymatic cleavage, namely by our group (Fonseca et al., 2011; Fonseca et al., 2013; Maia, Fonseca, et al., 2014).

While different chemical strategies have been reported for the incorporation of bioactive or crosslinking moieties in alginate polymers, many of them are biologically harmful, slow, and lack chemoselectivity (Kennedy et al., 2011; Kim & Koo, 2019). Recently, bio-orthogonal click chemistries have emerged as attractive alternative approaches, providing fast reaction rates in complex aqueous media, at physiologic pH and temperature (Scinto et al., 2021). In addition, there is now a set of click reactions that do not require the use of toxic reagents, as in early reports, which can be carried in the presence of cells, without compromising viability (Kim & Koo, 2019). Among these, strain-promoted azide-alkyne cycloaddition (SPAAC) is firmly established as a powerful and versatile click chemistry tool, widely used in the preparation, decoration, and assembly of polymeric structures (Guo et al., 2017; Jain et al., 2021; Li et al., 2021; Selegard et al., 2017; Takahashi et al., 2013). It involves the spontaneous and selective reaction of cyclooctyne derivatives with azide-bearing molecules, forming stable triazoles, only by mixing and stirring, without the need for catalysts or tightly controlled reaction conditions (Dommerholt et al., 2016; Li et al., 2021).

Herein, we hypothesized that SPAAC could be used to produce MMP-sensitive alginate hydrogels that could still undergo ionic crosslinking, improving the performance of these hydrogels as ECM-mimics (Fig. 1). Low amounts of bi-functional azido-modified PVGLIG peptides were grafted to cyclooctyne-alginate (ALG-K) to establish links between polymer chains, rather than form a network. This yielded soluble PVGLIG-alginate derivatives that were later converted into hydrogels via a secondary (ionic) crosslinking step, as envisaged. Alginate was also SPAAC-clicked with mono-functional azido-RGD peptides to promote cell adhesion. The peptide-modified derivatives were characterized in detail, and the response of 3D-cultured cells to cell responsive/instructive MMP-sensitive alginate hydrogels was assessed. To illustrate the applicability of the proposed hydrogels for the regeneration of soft tissue, like the dermis, we used dermal fibroblasts as model cell. While these materials may not fully replicate the complexity and functionality of the natural ECM, they offer significant advantages in terms of their well-defined composition and tunable properties, providing invaluable tools as ECM-like matrices for 3D cell culture.

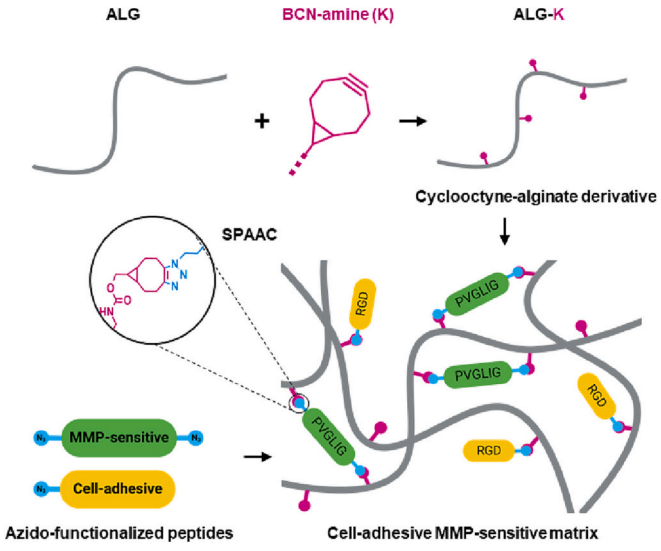

Fig. 1. SPAAC conjugation of azide-functionalized peptides to BCN-alginate (ALG-K) via copper free click reaction between azide and cyclooctyne groups (K), to yield cell responsive/instructive alginate conjugates with MMP-sensitive (PVGLIG) and cell-adhesive (RGD) domains.

2. Materials and methods

2.1. Production of cyclooctyne-alginate (Alg-K) derivatives

Ultrapure sodium alginate (Pronova UP LVM, FMC BioPolymers) with low viscosity (110 mPa.s at 1 wt% and 20 °C) and mannuronate-to-guluronate ratio of 51 % was used. ALG carboxyl groups were modified with N-(1*R*,8*S*,9*s*)-Bicyclo6.1.0non-4-yn-9-ylmethyloxycarbonyl-1,8-diamino-3,6-dioxaoctane (BCN-amine, Sigma-Aldrich) by carbodiimide chemistry. Briefly, ALG was dissolved (1 % w/v) in MES buffer saline (0.1 M MES, 0.3 M NaCl, pH 6.5) and EDC:COOH molar ratio of 1:20 were used to produce ALG-K derivatives. N-Hydroxysulfosuccinimide sodium salt (sulfo-NHS) and (3-dimethylaminopropyl)-N′-ethyl-carbodiimide hydrochloride (EDC) were sequentially added (1:2 M ratio) to the ALG solution. BCN-amine dissolved in dimethyl sulfoxide (DMSO) and deionized water (dH_2O) (5:2 v/v) was added in a 1.2 M excess to EDC. The reaction was performed under inert atmosphere (Ar) and room temperature (RT) for 20 h. To stop the reaction, hydroxylamine was added in equimolar ratio to EDC. Polymer solutions were dialyzed for 3 days in dH_2O with decreasing concentrations of NaCl (0.75–0 % w/v), freeze dried and stored (−20 °C). Control materials were produced following this protocol without BCN-amine addition.

2.2. ^{1}H Nuclear Magnetic Resonance (^{1}H NMR) analysis of ALG-K derivatives

Samples were dissolved at 0.8 % w/v in deuterium oxide (D_2O, Sigma-Aldrich) and 3-(trimethylsilyl)propionic-2,2,3,3-d4 acid sodium salt (TSP-d4, Euriso-top) was added as internal standard. Spectra were recorded on a BRUKER AVANCE III (400 MHz, 9.4 Tesla) NMR spectrometer and analyzed using Mnova software (version 11.0, Mestrelab Research). MD was determined by correlating the area of ALG peaks (δ = 4.561–4.369 ppm) with the new BCN peak (δ = 2.18–2.35 ppm), according to the following Eq. (1):

$$MD = \left(\frac{\frac{\int \delta BCN}{H_{\delta BCN}}}{\frac{\int \delta ALG}{H_{\delta ALG}} + \frac{\int \delta BCN}{H_{\delta BCN}}} \right) \times 100\ (\%) \quad (1)$$

where integrals correspond to the area of the peaks in a particular δ and H corresponds to the number of protons attributed to those same peaks.

2.3. Synthesis and characterization of azide-functionalized peptides

RGD-containing peptide sequence (GGGGRGDSP, U246KFF080-1/PE4635, GeneScript) and PVGLIG-containing peptide sequence (GGYGPVG↓LIGGK, 93083880005/PE0758, GeneScript) were modified with azide groups via their primary amines. Briefly, RGD or PVGLIG were dissolved in sodium bicarbonate buffer (pH 8.3) and NHS-C_3-azide in DMSO was added in 1:1 or 1:2.5 M ratio, respectively. The mixture was allowed to react for 4 h at RT with agitation. Azide incorporation was monitored by mass spectrometry (LC-MS/MS, Q-Exactive, Thermo

Scientific) by preparing samples in a 10/90 % v/v of sample and TFA 1 % solution, respectively. The mixture was then purified by ZipTip procedure and resuspended in FA 0.1 %. Data were analyzed using Xcalibur™ software (ThermoScientific).

2.4. Synthesis of PVGLIG-functionalized ALG-K by SPAAC

ALG-K solutions (1.5 % w/v in 0.9 % w/v NaCl) were prepared and allowed to react with RGD-N_3 or N_3-PVGLIG-N_3 overnight at RT with agitation. Formulations with different PVGLIG-crosslinking degrees were prepared with solutions containing final peptide concentrations of 0, 50, 125 and 250 μM N_3-PVGLIG-N_3 (P0, P50, P125 or P250, respectively).

2.5. Titration of free cyclooctyne groups in ALG hydrogels with fluorescent azido-tag

P0, P50, P125 or P250 were diluted in dH_2O down to 0.5 % w/v, plated and mixed (90/10 % v/v) with 3-azido-7-hydroxycoumarin (Coum-N_3, ChemiMart GmbH), which only becomes fluorescent following SPAAC reaction ($\lambda_{ex/em}$: 404/477 nm), at concentrations between 25 and 300 μM for 16 h. Fluorescence readings were obtained by endpoint reads every 5 min.

2.6. Attenuated Total Reflectance Fourier-transform infrared spectroscopy (ATR-FTIR) of PVGLIG-modified ALG-K

P0, P50, P125 or P250 samples were dialyzed for 3 days in dH_2O to remove any unreacted N_3-PVGLIG-N_3 peptide and freeze dried. ATR-FTIR spectra were acquired for lyophilized material (100 scans, 4 cm^{-1} resolution wavenumber range from 4000 to 400 cm^{-1}, Perkin-Elmer 2000). Spectra were analyzed using F. Menges "Spectragryph – optical spectroscopy software" (Version 1.2.13, 2019).

2.7. Triple size exclusion chromatography (SEC)

Triple-SEC of ALG-K formulations was used for quantification of molecular weight and intrinsic viscosity of modified and non-modified ALG-K (OMNISEC, Malvern Panalytical). Separations occurred at 30 °C in porous hydroxymethacrylate polymer columns (Viscotek A3000, A4000), using 0.5 M Na_2SO_4 as eluent, at a flow rate of 1 mL/min. Samples were dissolved in the eluent at a concentration of 2 mg/mL and prefiltered (0.45 μm) before injection. Samples were assayed in triplicate and data was analyzed with the OMNISEC software.

2.8. Production of 3D hydrogel discs by ionic gelation

Hydrogel discs were prepared by internal ionic gelation as previously described (Bidarra et al., 2014). Briefly, a precursor solution was prepared at a final concentration of 2 % w/v polymer in 0.9 % w/v NaCl. The solution was mixed with an aqueous suspension of sterile $CaCO_3$ (CalEssence® 70 Enhanced Purity PCC) at a $CaCO_3$/COOH molar ratio of 0.3 (Bidarra et al., 2014). Then, a fresh solution of glucone delta-lactone (GDL) was added to trigger gelation. The $CaCO_3$/GDL molar ratio was set at 0.25. Discs were prepared by dispensing 15 μL of the mixture into a Teflon-spacer-Teflon (500 μm height) sandwich system with a gelation time of 30 min.

2.9. Enzymatic sensitivity of PVGLIG-ALG-K conjugates

ALG, P0, P50, P125 or P250 hydrogel discs were prepared by internal ionic gelation as described above. Then, they were incubated at RT in collagenase type IV (200 units/L in HBSS) for 24 h. After incubation, discs were washed in HBSS overnight to remove all the unreacted collagenase and dissolved in EDTA (25 mM). The amount of free amines due to PVGLIG cleavage was monitored by reaction with fluorescamine by fluorescence reading at $\lambda_{ex/em}$: 400/460 nm.

2.10. Viscoelastic properties of ALG hydrogels

Hydrogels were collected at day 1 for mechanical characterization and punched into a 4 mm cylindrical shape. Rheological measurements were carried out at 37 °C using a Kinexus Pro rheometer (Malvern) and in a water-vapor saturated environment, using a plate-and-plate geometry (4 mm diameter, sandblasted surfaces) and compressed in 20 % of their original thickness to avoid slippage. The linear viscoelastic region (LVR) was determined by iteratively performing strain amplitude sweep and frequency sweep measurements. The shear moduli (G' and G'') and phase angle were obtained as average values of the LVR region in the amplitude strain sweeps (0.1–100 s^{-1} at 0.1 Hz).

2.11. 3D culture in SPAAC-functionalized PVGLIG/RGD-ALGK hydrogels

For the 3D cultures, primary Human dermal fibroblasts (neonatal, HDFn) were used. Cells were maintained in Dulbecco's Modified Eagle Medium (DMEM), supplemented with 10 % v/v fetal bovine serum and 1 % v/v penicillin/streptomycin (all from Gibco). For cell-laden hydrogels, ALG was previously partially oxidized with sodium periodate (at 1 % per monomer), as previously described (Evangelista et al., 2007; Torres et al., 2018), and only then the cyclooctyne moiety was grafted via carbodiimide chemistry with a final modification degree of 2.6 %. Formulations containing N_3-PVGLIG-N_3 (input amounts: 0, 50, 125, and 250 μM; reacted ON at 20 °C under stirring) or RGD-N_3 (input excess amount: 800 μM, reacted ON at 20 °C under stirring) were mixed in a 50/50 % v/v ratio prior cell-embedding and hydrogels were formed at a final polymer concentration of 2 % w/v in 0.9 % w/v NaCl. HDFn were added to the gel-precursor solution (10^7 cells/mL gel). Gelation was allowed to occur for 30 min at 37 °C.

2.12. Analysis of cell morphology and ECM production by immunofluorescence

Hydrogels were fixed with 4 % v/v paraformaldehyde in HBSS (20 min, RT) and permeabilized with a 0.2 % v/v Triton X-100 in HBSS (20 min, RT). For CLSM, samples were blocked in 1.5 % w/v bovine serum albumin (BSA) in HBSS (1 h, RT) with agitation and incubated with primary antibodies (1:100 dilution) rabbit anti-human fibronectin (FN, F3648, Sigma-Aldrich) and MMP14/MTP1-MMP (MAB9181), and Phalloidin-488 (Actin, 424,201, Biolegend, 1:100 dilution) ON, at 4 °C. On the following day, discs were incubated with secondary antibodies (Alexa 594 goat anti-mouse, Alexa 594 anti-rabbit, ThermoFisher Scientific, 1:500) and DAPI (nuclei, Merck, 3:500) for 1 h, and kept in HBSS, protected from light at 4 °C until further analysis. Samples were immersed in Vectashield™ during image acquisition by CLSM (Leica TCS SP5, Leica Microsystems). Image quantification was performed using Fiji software (Schindelin et al., 2012). To quantify the degree of cell-cell interconnectivity, an image analysis workflow was developed (in the format of a Fiji macro). The metric reflects, for each image and on average, how many pixels are connected. First, a maximum projection step is performed to convert the image stack to a 2D image, followed by a segmentation using the standard Otsu's method. All connected regions are then searched for to remove noise and/or artifacts. The average number of pixels in the identified connected regions is retrieved as the connectivity metric. Larger structures, even if in lesser numbers, lead to a higher connectivity metric. The results presented on graphs are normalized to the average values for the control samples.

2.13. Gene expression analysis

Hydrogels were collected at day 1, 7 and 14 of culture and dissolved in Trypsin-EDTA up to 10 min at 37 °C. Pellets were recovered by

suspension and centrifugation in phosphate buffered saline (PBS, pH 7.4). For mRNA expression quantification, RNA was extracted from hydrogels using the Quick-RNA MiniPrep (Zymo Research), as recommended by the manufacturer. Subsequently, RNA was reversed transcribed to single stranded cDNA using Takara cDNA synthesis kit. Quantitative Real-Time PCR (qRT-PCR) was carried out using source RNA from 4 biological replicas for the target genes *FN1, MMP2, MMP14* and for endogenous control GAPDH using as probe sets Hs.PT.58.40986315, Hs.PT.58.39114006, HS.PT.58.28187827 and Hs.PT.51.1940505 (Applied Biosystems and Integrated DNA Technologies), respectively. Samples were run in duplicate using TaqMan master mix in an ABI Prism 7000 Sequence Detection System under the following conditions: 95 °C for 20 s, followed by 40 cycles at 95 °C for 3 s and 60 °C for 30 s. The expression value for each target gene was normalized to GAPDH value for all the samples.

2.14. Cleavage of FRET-peptides by HDFn-secreted proteases

To analyze if the secretome of embedded cells contained active proteases capable of inducing PVGLIG cleavage, fluorescence resonance energy transfer (FRET) peptides were used (Maia, Barbosa, et al., 2014). As a control, a scrambled sequence (GIVPGL) less sensitive to protease cleavage was used. Conditioned media (CM) from HDFn cultures were collected on day 14 after 12 h of serum-starvation, and centrifuged to remove cell debris. Then, the CM were incubated with FRET-PVGLIG and FRET-GIVPL and the enzymatic cleavage of both peptides was estimated by measuring the increase in fluorescence ($\lambda_{ex/em}$ = 320/420 nm) after 24 h.

2.15. Statistical analysis

Statistical analysis was performed using GraphPad Prism software (GraphPad Software Inc., version 6.0). Data was analyzed by D'Agostino and Pearson omnibus normality test to assess the distribution of the

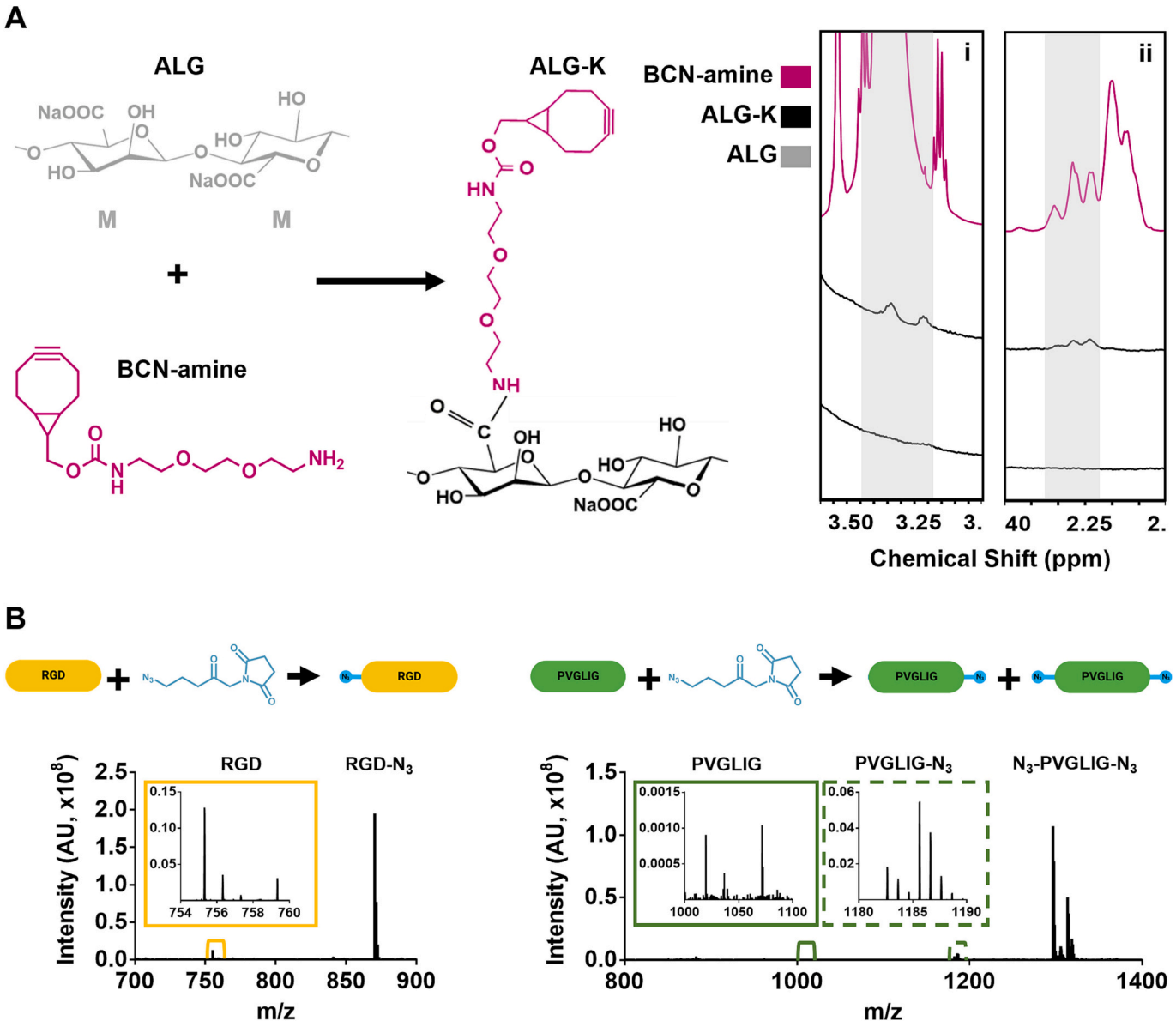

Fig. 2. (A) Schematic representation of the synthesis approach to produce the ALG-K derivative by grafting cyclooctyne (K) in the ALG backbone (two mannuronate monomers are presented, M) via carbodiimide chemistry, and characterization of the product by ^{1}H NMR spectroscopy. (B) Schematic representation of the chemical approach to incorporate N_3-moieties in RGD and PVGLIG peptides, and characterization by LC-MS/MS.

data. Welch's *t*-test was used for data with a normal distribution and non-parametric Mann-Whitney test was used to compare between groups that did not pass the normality test. Statistical differences are represented by * ($P < 0.05$), ** ($P < 0.01$) and *** ($P < 0.001$).

3. Results and discussion

In this work, cell responsive/instructive 3D matrices were produced by combining a cyclooctyne-alginate derivative with azido-containing bioactive peptides, namely the MMP-sensitive GGYGPVGLIGGK and the cell-adhesive GGGGRGDSP sequences, hereafter referred to as PVGLIG and RGD, respectively (Fig. 1). To do so, we started by incorporating SPAAC-clickable cyclooctyne moieties onto the alginate (ALG) backbone via carboxyl groups (COOH), reacting the natural polymer with the cyclooctyne containing BCN-amine (K), by conventional carbodiimide chemistry (Fig. 2A). The ^{1}H NMR analysis confirmed the successful incorporation of K into ALG, with the appearance of new peaks, particularly at 2.18–2.35 ppm and 3.34 ppm. The modification degree (MD) of ALG-K derivative was determined to be 3.49 % (Supplementary Fig. 1). A more detailed physicochemical characterization of ALG-K derivatives with different modification degrees is provided in (Neves et al., 2023).

Then, in order to provide SPAAC-reactivity to PVGLIG and RGD peptides, these were modified to incorporate azide (N_3) groups. The MMP-sensitive oligopeptide used herein (GGYGPVG↓LIGGK) included the MMP-cleavable substrate PVG↓LIG, where the cleavage site (represented by ↓) is the peptide bond between glycine (G) and leucine (L) residues. Besides the N-terminal amine, the sequence presents another reactive primary amine in the lysine (K) motif, which is located near the C-terminus. The target MMP-sensitive motif was flanked by glycine (G) residues, which were used as spacers to improve exposure of the bioactive sequence. In both peptides, the primary amines were functionalized with azide groups via reaction with NHS-C_3-azide, yielding SPAAC-reactive N_3-PVGLIG-N_3 (bi-functional, N-termini and lysine residues) conjugates and RGD-N_3 (monofunctional, N-terminus) (Fig. 2B). The successful production of azido-peptides was proved by LC-MS/MS, where the modified peptides showed an increase in the mass/charge ratio (m/z) as compared to unmodified peptides. Since RGD

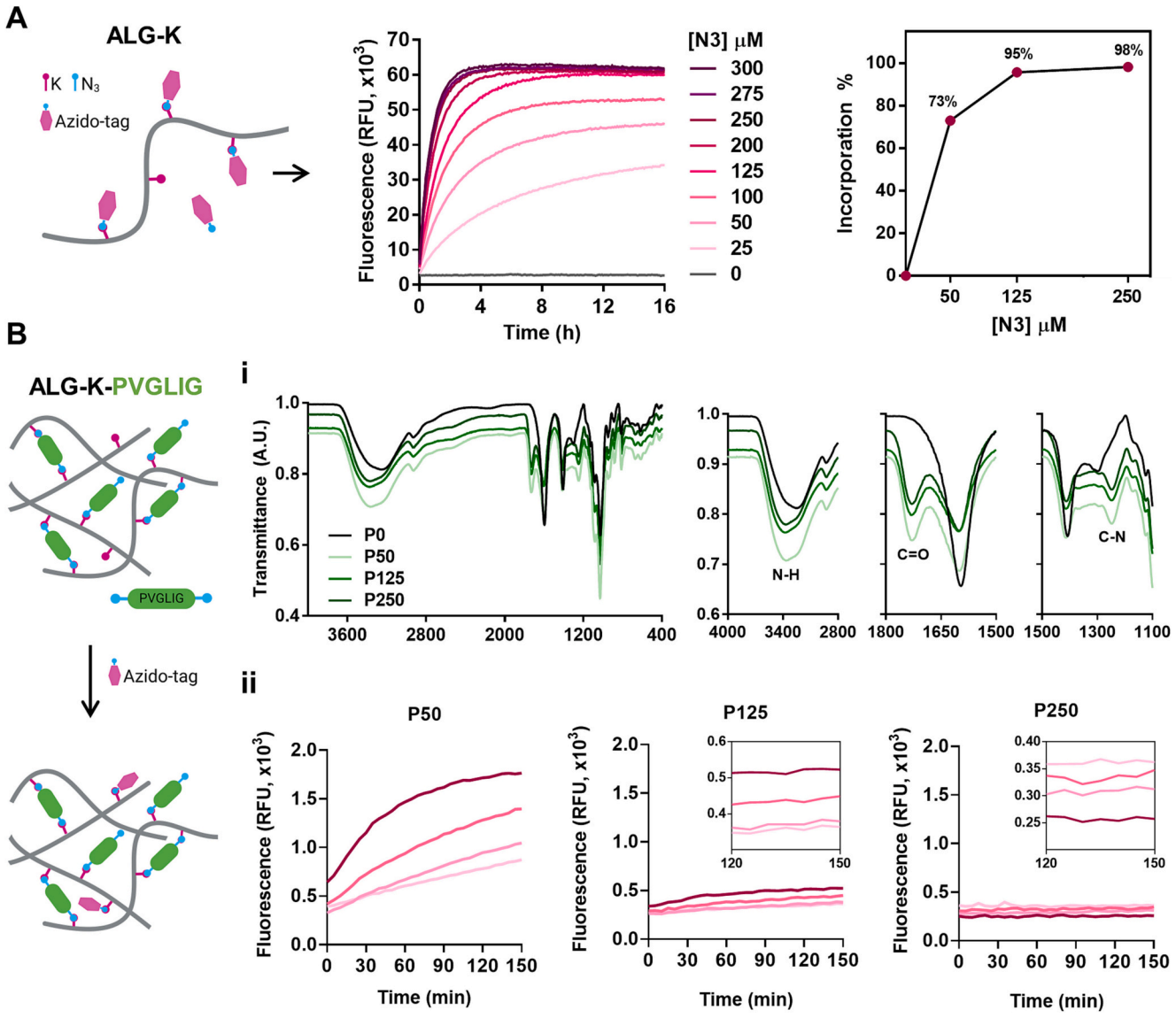

Fig. 3. SPAAC reactivity of ALG-K and ALG-K-PVGLIG. (A) SPAAC reactivity of ALG-K derivative reactivity towards an azido-containing fluorescent tag, showing an increase in fluorescence with azide concentrations up to 300 μM (100 %), and calculated percentage of incorporation for different concentrations of available N_3-tag. (B) Incorporation of PVGLIG onto ALG-K and SPAAC reactivity of ALG-K-PVGLIG groups. (Bi) ATR-FTIR spectra showing the appearance of new peaks corresponding to the grafted PVGLIG peptide in ALG-K formulations. (Bii) Titration of the remaining free cyclooctyne groups in ALG-K-PVGLIG formulations.

contained only one free reactive amine at the N-termini, it was expected that, upon reaction, the unmodified RGD peptide would disappear as the mono-functionalized species were formed. Indeed, the strong peak at 870.38 m/z corresponding to RGD-N_3 indicates an increase of ~112 Da, corresponding to the new azido-containing group ($N_3C_4OH_6$, 112.11 g/mol), in relation to unmodified RGD (758.74 m/z), which was residual (yellow inset). The double azidation of PVGLIG was also successful with residual to near zero presence of non-modified (PVGLIG, 1074.24 m/z) or mono-functionalized (PVGLIG-N_3, 1185.63 m/z) species (green insets). As can be observed in the spectrum, strong peaks occur in the 1296.68 m/z region, corresponding to the bi-functionalized N_3-PVGLIG-N_3, now containing one azido-group on both ends of the peptide sequence.

To assess its SPAAC-clicking potential, ALG-K (0.5 % w/v) was reacted with a pro-fluorescent azido-coumarin, which affords a highly fluorescent triazole product only upon SPAAC-reaction, eliminating the need for probe washout. The fluorogenic azido-coumarin was used as a surrogate of an azido-peptide, and different concentrations (from 25 to 300 μM) were tested to monitor reaction kinetics over 16 h. Depending on the initial azido-coumarin concentration, the fluorogenic reactions followed pseudo-first order (lower concentrations) or second order profiles (higher concentrations), as previously reported for SPAAC reactions (Kim & Koo, 2019; Mbua et al., 2011). By looking at the kinetic profiles in Fig. 3A, it can be concluded that the maximum incorporation (saturation) occurred around 300 μM, the percentage of incorporation peptide increases as the concentration of azido-coumarin increased, and no significant differences were observed above 250 μM.

Taking this into account, for SPAAC-reactions with N_3-PVGLIG-N_3 the amount of input peptide was varied within the range of 50 to 250 μM. The reactions were carried out for at least 12 h, to guarantee reaching values close to the plateau in all cases. PVGLIG incorporation was confirmed by ATR-FTIR analysis in lyophilized samples (Fig. 3 Bi). In the spectra, it is possible to see the appearance of new peaks around 3411 cm^{-1}, corresponding to N—H stretching vibrations from the secondary amides present in the peptide, which partially overlapped with the broad O—H region (3000–3700 cm^{-1}). Additionally, new peaks at 1260 cm^{-1} corresponding to C—N stretching vibrations and at 1735 cm^{-1}, corresponding to carbonyl groups were detected. After demonstrating that PVGLIG had successfully been grafted into ALG-K, a titration of free K groups in ALG-K-PVGLIG formulations (P50, P125 and P250) immediately after reaction was performed with the pro-fluorescent azido-coumarin reporter. Fig. 3 Bii shows the kinetic profiles and the relative amount of free K groups for all of them. The P50 formulation is the one presenting higher SPAAC reactivity, which reflects a higher amount of free K groups. The P125 formulation presents much lower reactivity, consistent with higher incorporation and eventual double-end grafting, (meaning that each incorporated peptide occupied two K groups). The P250 formulation presents nearly no SPAAC reactivity, consistent with the almost absence of available K groups.

The PVGLIG-ALG-K conjugates were also analyzed by Triple-SEC to confirm the ability of bi-functional PVGLIG peptides of establishing crosslinks between ALG-K chains (Fig. 4 and Table 1). Fig. 4 shows the low angle light scattering (LALS) chromatograms for unmodified ALG, ALG-K (P0) and PVGLIG-ALG conjugates (P50, P125, P250), which allow the detection of larger components or potential aggregates within samples, even if they exist in low concentration. Compared to ALG, the ALG-K (P0) sample presented higher molecular weight (lower retention volume, Vr), which may be explained by the presence of the additional K groups and by the eventual establishment of inter/intra-chain hydrophobic associations between those groups (Babak et al., 2000; Galant et al., 2006; Tan et al., 2018). Compared to P0, the P50 and P125 samples showed a slightly earlier elution time and a non-resolved shoulder at the higher molecular weight region (lower Vr). This suggests the presence of higher order molecular weight species, supporting the formation of peptide-mediated crosslinks. Notably, the elution

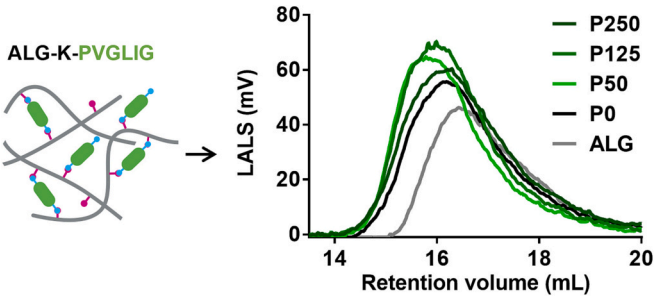

Fig. 4. Triple-GPC/SEC chromatogram for unmodified ALG, ALG-K derivative and ALG-K grafted with different amounts of PVGLIG. Table 1 presents the molecular data obtained for the series of ALG samples. Depicted values include the molecular weight moments (M_n, M_w), the polydispersity (PDI), the intrinsic viscosity ([η]), and hydrodynamic radius (R_h).

Table 1
Data derived from Triple-GPC/SEC analysis for ALG, ALG-K (P0) and ALG-K-PVGLIG (P50, P125, P250) samples (n = 3 independent experiments).

	ALG	P0	P50	P125	P250
M_n (kDa)	107 ± 14	113 ± 40	123 ± 19	116 ± 64	113 ± 30
M_w (kDa)	204 ± 13	289 ± 12	393 ± 31	380 ± 33	322 ± 13
PDI	1.9	2.6	3.2	3.3	2.9
[η] (dL/g)	6.8 ± 0.0	7.1 ± 0.1	7.6 ± 0.2	7.4 ± 0.1	7.2 ± 0.3
Rh_w (nm)	26.2 ± 0.6	28.9 ± 0.8	32.1 ± 1.4	31.6 ± 1.1	29.9 ± 0.8

profile of the P250 sample is closer to P0 than to the other conjugates. Most likely, the much higher amount of peptide available for reacting favors competition for the free K groups, resulting mainly in grafting by one end and not by both ends. As a result, instead of establishing effective crosslinks, the grafted peptide will be mainly in pending form. The data in Table 1 confirm these trends: the P50 and P125 samples showed higher (and more polydisperse) molecular weight (Mw), intrinsic viscosity (η), and molecular size (R_h) than P0, while P250 is similar to P0.

To analyze the susceptibility of the bound peptides to proteolytic degradation, PVGLIG-ALG-K hydrogels were prepared by secondary ionic crosslinking and incubated with collagenase for 24 h (Fig. 5). Proteolysis was evaluated in the presence of fluorescamine, which becomes fluorescent upon reaction with free amines. These are not present in the azide-modified peptide (as shown in Fig. 2B) but will become exposed as N-termini amines upon cleavage. PVGLIG-ALG-K hydrogels incubated in buffer with no collagenase, P0 hydrogels (ALG-K without PVGLIG) and unmodified ALG hydrogels were used as controls. The graph in Fig. 5 depicts the net values obtained for the ALG-K-PVGLIG samples, i.e., after blank (buffer) subtraction. An increase in fluorescence was detected in P0 samples as compared to ALG, suggesting that the hydrophobic K groups may slightly interfere with the assay, either by locally sequestering collagenase (which has free amines) via hydrophobic interactions, or by directly interacting with fluorescamine. Still, in ALG-K-PVGLIG samples, the number of free amines increased with the amount of grafted peptide, demonstrating that the PVGLIG moieties remained protease-sensitive after conjugation.

For 3D cell culture studies using HDFn, both peptides were SPAAC-clicked on slightly oxidized (1 %) alginate ALG-K, a previously optimized formulation (Evangelista et al., 2007; Torres et al., 2018) used herein as the benchmark, as too restrictive hydrogels act as barriers for cells despite MMP-sensitivity and presence of adhesion sites (Bott et al., 2010). The aim was to show that the incorporation of protease-sensitive crosslinking peptides would further improve the performance of this (partially) degradable alginate hydrogel as an ECM-like matrix for 3D culture. To guarantee that the amount of RGD remained constant in all formulations, the two peptides were SPAAC-clicked to ALG-K in individual reactions to produce ALG-K-RGD and ALG-K-PVGLIG. The two

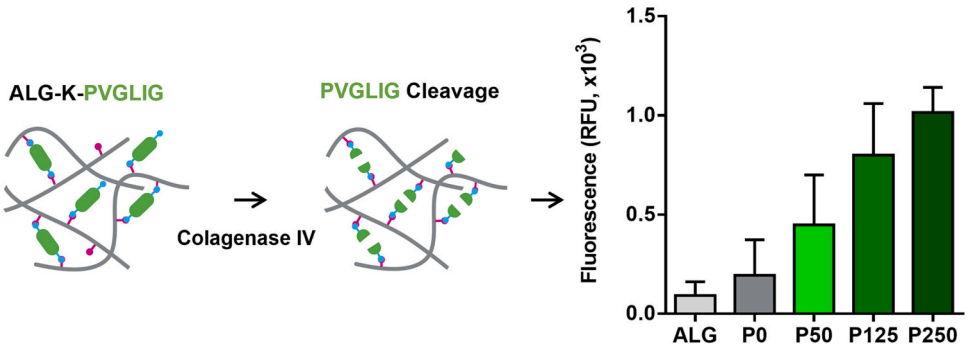

Fig. 5. Susceptibility of grafted PVGLIG to cleavage by collagenase IV, as estimated by the fluorescamine assay, which measures the total amount of free amines in peptides, which become exposed after enzymatic cleavage (n = 3 independent experiments).

derivatives were then combined at 1:1 ratio to yield gel-precursor solution with the same amount of RGD (grafted amount ~ 200 μM) and variable amounts of PVGLIG (50, 125 and 250 μM).

Hydrogels were formed by secondary ionic crosslinking and we used a total polymer concentration of 2 % w/v to provide soft hydrogels (G´< 1 kPa), as previously optimized for other systems developed by us for dermal tissue regeneration (Feijao et al., 2021; Neves et al., 2015). The rheological analysis of the different formulations showed hydrogels to be similar and relatively soft (700 Pa < G´< 900 Pa) (Fig. 6A). Even though not significant, there was a tendency for G' to increase from $P0_{ox}$ to $P50_{ox}$ and $P125_{ox}$, which was reversed in $P250_{ox}$, supporting the establishment of peptide-crosslinks when PVGLIG was used at 50 and 125 μM, as suggested by the Triple-SEC results. Fibroblasts embedded in these formulations showed high cell viability, as observed by the Live/Dead assay (Fig. 6B). On day 1, cells showed a compact spherical shape in all formulations, which reflects the physical restriction imposed by the polymeric network (Fig. 6C). The presence of short cytoplasmatic protrusions around the cell suggests cell-matrix interactions via RGD-mediated integrin engagement, as previously described by us (Fonseca et al., 2011; Maia, Fonseca, et al., 2014; Neves et al., 2015) and others (Jain et al., 2021; Rowley & Mooney, 2002). On day 14, cells were able to adopt an elongated morphology and spread over time in the partially degradable $P0_{ox}$, as anticipated, as well as in all the PVGLIG-grafted formulations. The graph in Fig. 6D depicts the degree of cell-cell interconnections for the different formulations. While in this study a relatively high cell density was used, which inherently favors cell-cell interactions, there were clear differences among the tested hydrogels. The best results were obtained for the $P125_{ox}$ formulation, where cells showed an increased ability to interact with neighboring cells and form complex multicellular networks. This suggests that while the partially degradable $P0_{ox}$ hydrogels provides per se a cell permissive matrix, the presence of crosslinking PVGLIG peptides further improves their properties, as hypothesized. This also provides a cell-driven proteolytic mechanism for matrix remodeling, which is more biologically relevant.

In MMP-sensitive hydrogels the enzymatic cleavage of the double-end grafted PVGLIG peptides is expected to allow cells to locally remodel the polymeric network and help them in overcoming the physical confinement. Notably, since hydrogels are stabilized by ionic crosslinking, their macrostructural integrity was preserved over culture and remodeling was essentially confined to the pericellular space, similar to what occurs in native tissues (Holmbeck & Szabova, 2006; Sternlicht & Werb, 2001) and in other artificial ECMs (Daviran et al., 2018; Schultz et al., 2015). In future studies it would be interesting to characterize the morphological properties of the different hydrogel networks and how they change along the culture. Overall, the formation of multicellular networks appears to result from the dynamic balance between cell-matrix and cell-cell interactions and (facilitated) motility conditions (da Rocha-Azevedo & Grinnell, 2013).

The behavior of dermal fibroblasts in $P125_{ox}$ hydrogels, the ones showing the best outcome, was analyzed in more detail. As depicted in Fig. 7A, the embedded HDFn were able to produce their own ECM, as shown by the deposition of fibronectin at the pericellular space. The organization of a FN-rich fibrillar matrix could be observed in regions of clustered cells along cell extensions, primarily beneath and along their margins, as previously reported (da Rocha-Azevedo & Grinnell, 2013). Accordingly, *FN1 mRNA expression* levels increased significantly from day 1 and 7 to day 14 (Fig. 7A). Cleavage of PVGLIG domains can be mediated by secreted and/or membrane bound matrix metalloproteinases (MMPs), including MMP2 and MMP14, respectively, as previously reported (Fonseca, Gomes, et al., 2014). To confirm the ability of 3D-cultured cells to cleave the PVGLIG sequence, conditioned medium was collected and incubated with a highly sensitive FRET-PVGLIG probe (Fig. 7B) (Maia, Barbosa, et al., 2014). This substrate (Abz-GGYGPVGYLIGGK-Q-EDDnp) has a fluorophore (Abz) and a quencher (EDDnp) attached to either end. In the intact molecule, fluorescence resonance energy transfer between the donor/acceptor groups leads to low fluorescence. When the peptide is cleaved, the groups become separated and the fluorescence increases, as observed herein upon incubation with the secretome of cells embedded in $P125_{ox}$ hydrogels. The scrambled peptide sequence FRET-GIVGPL, protease-sensitive but less specific (Maia, Barbosa, et al., 2014), was also cleaved to a lower extent. The expression of MMP14 at protein level was confirmed by immunostaining (Fig. 7C) of whole-mounted samples and by gene expression. Finally, the mRNA expression levels of *MMP2* and *MMP14* also increased over time, particularly for MMP2 that presented a significant increase at day 7 and 14 in comparison to day 1 (Fig. 7D).

Overall, this study provides a comprehensive description of the design, synthesis, and characterization of innovative ECM-like biomaterials, specifically focusing on their physicochemical properties and biological performance. The response of dermal fibroblasts to the developed hydrogels was studied as a proof-of-concept, considering that alginate is by far the most commonly used biomaterial among other bioproducts with wound healing properties (Barbu et al., 2021). However, these materials have other potential applications in TE, as they mimic fundamental characteristics found in all types of various native ECMs. By incorporating other bioactive peptides, such as growth factor mimetics, into the hydrogel matrix using SPPAC, tissue-specific environments can be recreated. This opens possibilities for guiding cell differentiation and enhancing the regeneration of various tissue types. Importantly, the translation of these biomaterials into clinical applications necessitates regulatory approval, which is a crucial step. Ensuring consistency and reproducibility of the manufacturing process at larger scales will be important. Additionally, demonstrating the safety and efficacy of these materials through rigorous preclinical and clinical studies is essential. These studies will provide a better understanding of their interactions with living tissues and help identify any potential adverse effects. Classification of the peptide-modified alginate hydrogels under existing regulatory frameworks must also be considered.

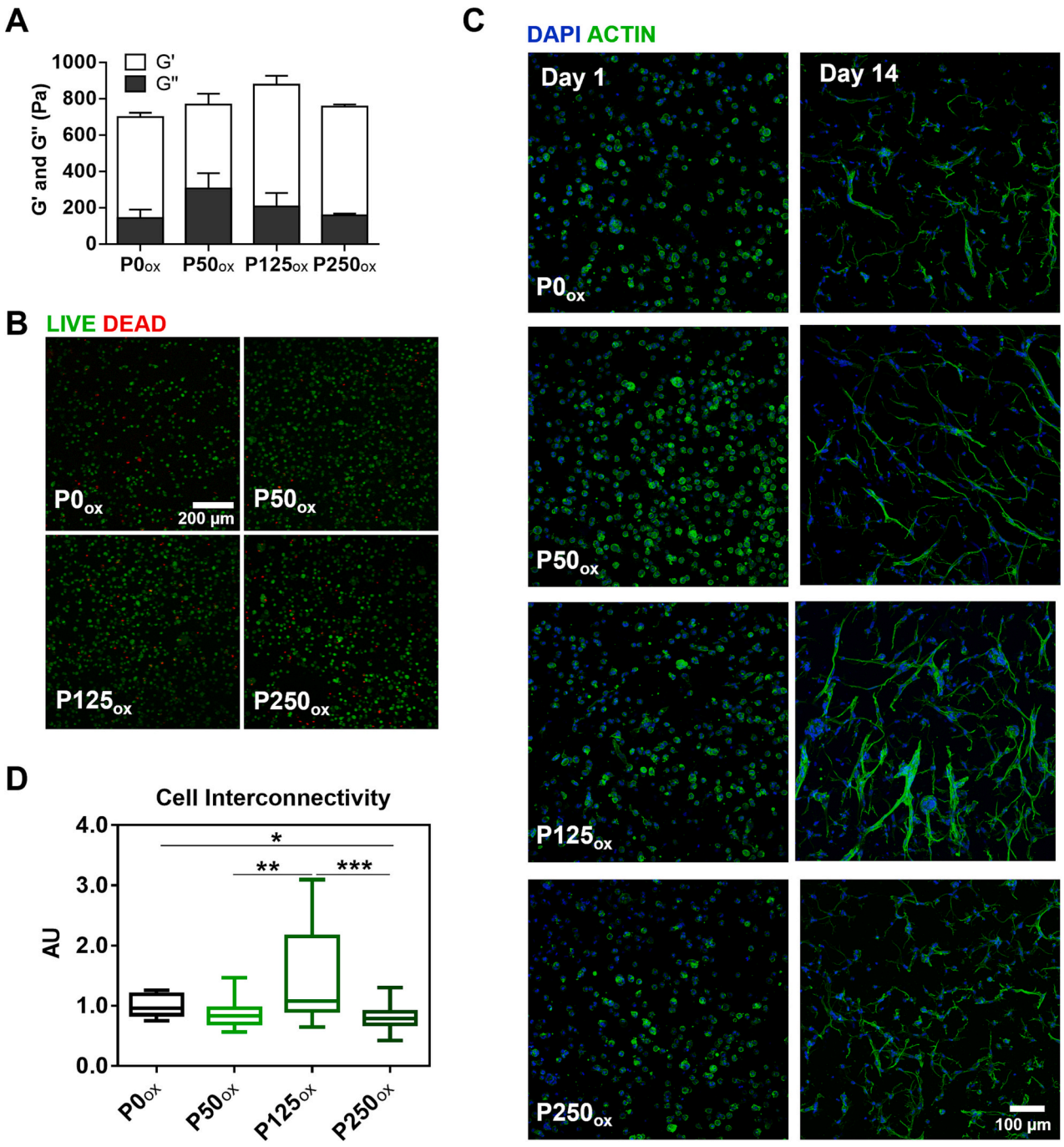

Fig. 6. Mechanical properties and cell viability and spreading in ionically crosslinked PVGLIG/RGD-oxALG-K hydrogels. (A) Elastic and viscous components of the shear moduli of hydrogels on day 1 showing a tendency for PVGLIG-containing hydrogels to present slightly increased stiffness (n = 3). (B) Live/Dead assay of embedded HDFn on day 1. (C) Representative CLSM images of actin staining showing HDFn morphology throughout culture time. (D) Degree of cell-cell interconnectivity measured by analysis of cell spreading and organization from CLSM images (n = 3 independent experiments). Statistical differences are represented by * ($P < 0.05$), ** ($P < 0.01$) and *** ($P < 0.001$).

Depending on their intended use, the hydrogels may fall into different categories, such as medical devices or combination products. Understanding and complying with the specific requirements applicable to these categories will be vital for successful regulatory approval.

In summary, this study contributes to the field by presenting innovative biomaterials with many different potential applications in TE. However, before these materials can be widely utilized in clinical settings, further research, regulatory considerations, and thorough evaluation of their safety and efficacy are necessary.

4. Conclusions

In this work, we report the successful synthesis of MMP-sensitive alginate partially crosslinked with PVGLIG peptides via SPAAC click-chemistry, which can still form hydrogels by secondary ionic crosslinking. The combination of SPAAC-clicked MMP-sensitive (PVGLIG) and cell adhesive (RGD) peptides in hydrolytically sensitive ALG generated multifunctional cell responsive/instructive 3D matrices, which supported cell viability, ECM production and cell organization into tissue-like interconnected networks. The amounts of each

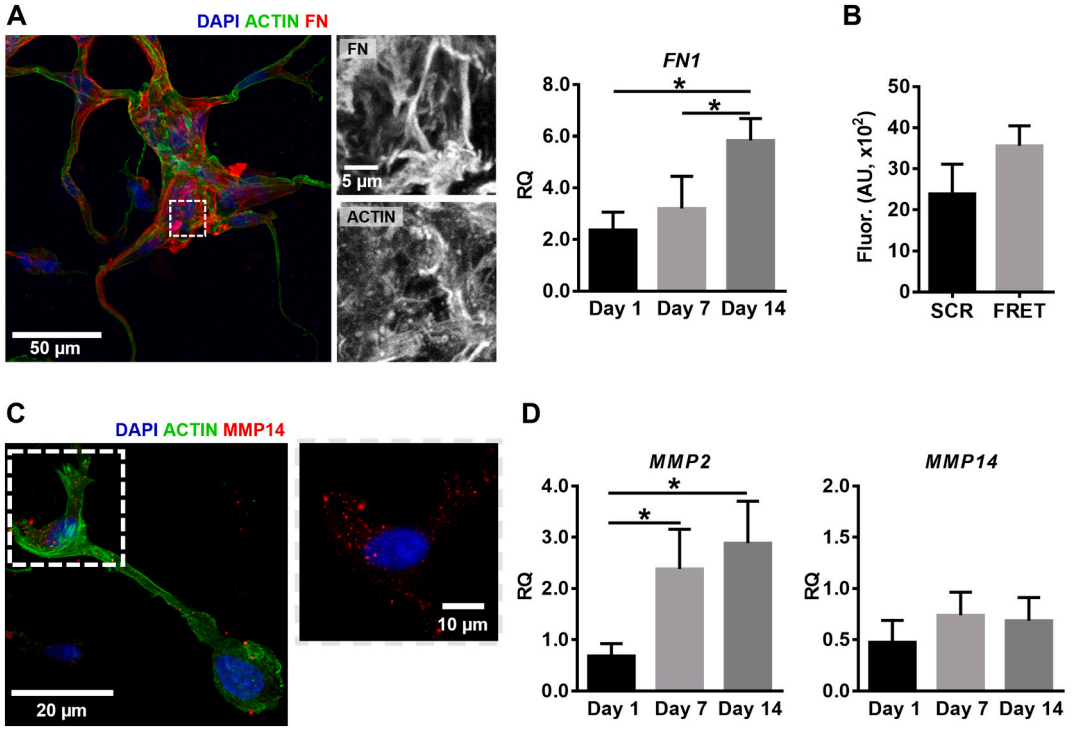

Fig. 7. ECM and MMP expression in HDFn-laden $P125_{ox}$ hydrogels. A) Fibronectin immuno-staining on day 14, showing extracellular deposition, and *FN* gene expression throughout culture time. (B) Cleavage of PVGLIG by compounds present in the secretome of cells cultured for 14 days. (C) MMP14 staining showing the presence of this protease at the cell surface on day 14. (D) *MMP2* and *MMP14* gene expression throughout culture time.

component can be easily and individually changed to tune hydrogel's biochemical properties, and the total amount of polymer or crosslinking density allows tuning hydrogel's mechanical properties. Thus, while these materials may not fully replicate the complexity and functionality of the natural ECM, they offer valuable advantages in terms of their well-defined composition and tunable properties. Overall, our approach provides a versatile platform to build customizable alginate matrices for 3D cell culture, recapitulating key features of native ECMs.

Supplementary data to this article can be found online at https://doi.org/10.1016/j.carbpol.2023.121226.

Funding

This work was supported by project EndoSWITCH (PTDC/BTM-ORG/5154/2020) funded by FCT (Portuguese Foundation for Science and Technology). The authors thank FCT for CCB's IF research position (Grant No: IF/00296/2015), MIN's scholarship (Grant No: SFRH/BD/129855/2017 and COVID/BD/151886/2022), MVM's scholarship (Grant No: SFRH/BD/10184/2022), and SJB's research contract DL 57/2016/CP1360/CT0006.

CRediT authorship contribution statement

MIN: scientific conceptualization, experimental design, bench work, data collection and analysis, manuscript writing. MVM: scientific conceptualization, experimental design, bench work, data collection and analysis, manuscript writing. SJB: qPCR data collection and analysis. LM: co-supervision of the work, manuscript revision. CCB: scientific conceptualization, experimental design, supervision of the work, manuscript revision.

Declaration of competing interest

The authors declare that they have no known competing financial interests or personal relationships that could have appeared to influence the work reported in this paper.

Data availability

All data needed to evaluate the conclusions in the paper are present in the paper and/or the Supplementary Information. All raw/processed data are available upon reasonable request addressed to the corresponding author.

Acknowledgments

The authors acknowledge the support of i3S Scientific Platforms: "Bioimaging" member of the PPBI (Grant No: PPBI-POCI-01-0145-FEDER-022122), "Biointerfaces and Nanotechnology" (Grant No: UID/BIM/04293/2019), the "Proteomics Scientific Platform", in particular Hugo Osório, financed by the Portuguese Mass Spectrometry Network, integrated in the National Roadmap of Research Infrastructures of Strategic Relevance (ROTEIRO/0028/2013; LISBOA-01-0145-FEDER-022125). The authors also acknowledge Paulo Aguiar, Group Leader of Neuroengineering and Computational Neuroscience Group at i3S for the development of the Fiji macro for the quantification of cell-cell interconnectivity degree. Finally, the authors acknowledge the Laboratory for Structural Elucidation (LAE) and the Image, Microstructure and Microanalysis Unit (IMCROS) from the Materials Centre of the University of Porto (CEMUP).

References

Babak, V. G., Skotnikova, E. A., Lukina, I. G., Pelletier, S., Hubert, P., & Dellacherie, E. (2000). Hydrophobically associating alginate derivatives: Surface tension properties of their mixed aqueous solutions with oppositely charged surfactants. *Journal of Colloid and Interface Science, 225*(2), 505–510.

Barbu, A., Neamtu, B., Zăhan, M., Iancu, G. M., Bacila, C., & Mireşan, V. (2021). Current trends in advanced alginate-based wound dressings for chronic wounds. *Journal of Personalized Medicine, 11*(9).

Bidarra, S. J., Barrias, C. C., Fonseca, K. B., Barbosa, M. A., Soares, R. A., & Granja, P. L. (2011). Injectable in situ crosslinkable RGD-modified alginate matrix for endothelial cells delivery. *Biomaterials, 32*(31), 7897–7904.

Bidarra, S. J., Barrias, C. C., & Granja, P. L. (2014). Injectable alginate hydrogels for cell delivery in tissue engineering. *Acta Biomaterialia, 10*(4), 1646–1662.

Bott, K., Upton, Z., Schrobback, K., Ehrbar, M., Hubbell, J. A., Lutolf, M. P., & Rizzi, S. C. (2010). The effect of matrix characteristics on fibroblast proliferation in 3D gels. *Biomaterials, 31*(32), 8454–8464.

Cao, L., Lu, W., Mata, A., Nishinari, K., & Fang, Y. (2020). Egg-box model-based gelation of alginate and pectin: A review. *Carbohydrate Polymers, 242*, Article 116389.

Daviran, M., Longwill, S. M., Casella, J. F., & Schultz, K. M. (2018). Rheological characterization of dynamic remodeling of the pericellular region by human mesenchymal stem cell-secreted enzymes in well-defined synthetic hydrogel scaffolds. *Soft Matter, 14*(16), 3078–3089.

Dommerholt, J., Rutjes, F. P. J. T., & van Delft, F. L. (2016). Strain-promoted 1,3-dipolar cycloaddition of cycloalkynes and organic azides. *Topics in Current Chemistry, 374*(2), 16.

Evangelista, M. B., Hsiong, S. X., Fernandes, R., Sampaio, P., Kong, H. J., Barrias, C. C., … Granja, P. L. (2007). Upregulation of bone cell differentiation through immobilization within a synthetic extracellular matrix. *Biomaterials, 28*(25), 3644–3655.

Feijao, T., Neves, M. I., Sousa, A., Torres, A. L., Bidarra, S. J., Orge, I. D., Carvalho, D. T. O., & Barrias, C. C. (2021). Engineering injectable vascularized tissues from the bottom-up: Dynamics of in-gel extra-spheroid dermal tissue assembly. *Biomaterials, 279*, Article 121222.

Fonseca, K. B., Bidarra, S. J., Oliveira, M. J., Granja, P. L., & Barrias, C. C. (2011). Molecularly designed alginate hydrogels susceptible to local proteolysis as three-dimensional cellular microenvironments. *Acta Biomaterialia, 7*(4), 1674–1682.

Fonseca, K. B., Gomes, D. B., Lee, K., Santos, S. G., Sousa, A., Silva, E. A., … Barrias, C. C. (2014). Injectable MMP-sensitive alginate hydrogels as hMSC delivery systems. *Biomacromolecules, 15*(1), 380–390.

Fonseca, K. B., Granja, P. L., & Barrias, C. C. (2014). Engineering proteolytically-degradable artificial extracellular matrices. *Progress in Polymer Science, 39*(12), 2010–2029.

Fonseca, K. B., Maia, F. R., Cruz, F. A., Andrade, D., Juliano, M. A., Granja, P. L., & Barrias, C. C. (2013). Enzymatic, physicochemical and biological properties of MMP-sensitive alginate hydrogels. *Soft Matter, 9*(12), 3283.

Galant, C., Kjøniksen, A.-L., Nguyen, G. T. M., Knudsen, K. D., & Nyström, B. (2006). Altering associations in aqueous solutions of a hydrophobically modified alginate in the presence of β-cyclodextrin monomers. *The Journal of Physical Chemistry B, 110*(1), 190–195.

Guo, C., Kim, H., Ovadia, E. M., Mourafetis, C. M., Yang, M., Chen, W., & Kloxin, A. M. (2017). Bio-orthogonal conjugation and enzymatically triggered release of proteins within multi-layered hydrogels. *Acta Biomaterialia, 56*, 80–90.

Holmbeck, K., & Szabova, L. (2006). Aspects of extracellular matrix remodeling in development and disease. *Birth Defects Research. Part C, Embryo Today, 78*(1), 11–23.

Jain, E., Neal, S., Graf, H., Tan, X., Balasubramaniam, R., & Huebsch, N. (2021). Copper-free azide–alkyne cycloaddition for peptide modification of alginate hydrogels. *ACS Applied Bio Materials, 4*(2), 1229–1237.

Kennedy, D. C., McKay, C. S., Legault, M. C., Danielson, D. C., Blake, J. A., Pegoraro, A. F., … Pezacki, J. P. (2011). Cellular consequences of copper complexes used to catalyze bioorthogonal click reactions. *Journal of the American Chemical Society, 133*(44), 17993–18001.

Kim, E., & Koo, H. (2019). Biomedical applications of copper-free click chemistry: In vitro, in vivo, and ex vivo. *Chemical Science, 10*(34), 7835–7851.

Li, K., Fong, D., Meichsner, E., & Adronov, A. (2021). A survey of strain-promoted azide–alkyne cycloaddition in polymer chemistry. *Chemistry – A European Journal, 27*(16), 5057–5073.

Loffek, S., Schilling, O., & Franzke, C. W. (2011). Biological role of matrix metalloproteinases: A critical balance. *The European Respiratory Journal, 38*(1), 191–208.

Lueckgen, A., Garske, D. S., Ellinghaus, A., Mooney, D. J., Duda, G. N., & Cipitria, A. (2020). Dual alginate crosslinking for local patterning of biophysical and biochemical properties. *Acta Biomaterialia, 115*, 185–196.

Maia, F. R., Barbosa, M., Gomes, D. B., Vale, N., Gomes, P., Granja, P. L., & Barrias, C. C. (2014). Hydrogel depots for local co-delivery of osteoinductive peptides and mesenchymal stem cells. *Journal of Controlled Release, 189*, 158–168.

Maia, F. R., Fonseca, K. B., Rodrigues, G., Granja, P. L., & Barrias, C. C. (2014). Matrix-driven formation of mesenchymal stem cell-extracellular matrix microtissues on soft alginate hydrogels. *Acta Biomaterialia, 10*(7), 3197–3208.

Mbua, N. E., Guo, J., Wolfert, M. A., Steet, R., & Boons, G. J. (2011). Strain-promoted alkyne-azide cycloadditions (SPAAC) reveal new features of glycoconjugate biosynthesis. *Chembiochem, 12*(12), 1912–1921.

Neves, M. I., Bidarra, S. J., Magalhães, M. V., Torres, A. L., Moroni, L., & Barrias, C. C. (2023). Microstructured click hydrogels for cell contact guidance in 3D. *Materials Today Bio, 19*, Article 100604.

Neves, M. I., Moroni, L., & Barrias, C. C. (2020). Modulating alginate hydrogels for improved biological performance as cellular 3D microenvironments. *Frontiers in Bioengineering and Biotechnology, 8*(665).

Neves, S. C., Gomes, D. B., Sousa, A., Bidarra, S. J., Petrini, P., Moroni, L., … Granja, P. L. (2015). Biofunctionalized pectin hydrogels as 3D cellular microenvironments. *Journal of Materials Chemistry B, 3*(10), 2096–2108.

da Rocha-Azevedo, B., & Grinnell, F. (2013). Fibroblast morphogenesis on 3D collagen matrices: The balance between cell clustering and cell migration. *Experimental Cell Research, 319*(16), 2440–2446.

Rowley, A. T., Nagalla, R. R., Wang, S. W., & Liu, W. F. (2019). Extracellular matrix-based strategies for immunomodulatory biomaterials engineering. *Advanced Healthcare Materials, 8*(8), Article e1801578.

Rowley, J. A., Madlambayan, G., & Mooney, D. J. (1999). Alginate hydrogels as synthetic extracellular matrix materials. *Biomaterials, 20*(1), 45–53.

Rowley, J. A., & Mooney, D. J. (2002). Alginate type and RGD density control myoblast phenotype. *Journal of Biomedical Materials Research, 60*(2), 217–223.

Schindelin, J., Arganda-Carreras, I., Frise, E., Kaynig, V., Longair, M., Pietzsch, T., … Cardona, A. (2012). Fiji: An open-source platform for biological-image analysis. *Nature Methods, 9*(7), 676–682.

Schultz, K. M., Kyburz, K. A., & Anseth, K. S. (2015). Measuring dynamic cell-material interactions and remodeling during 3D human mesenchymal stem cell migration in hydrogels. *Proceedings of the National Academy of Sciences of the United States of America, 112*(29), E3757–E3764.

Scinto, S. L., Bilodeau, D. A., Hincapie, R., Lee, W., Nguyen, S. S., Xu, M., Am Ende, C. W., Finn, M. G., Lang, K., Lin, Q., Pezacki, J. P., Prescher, J. A., Robillard, M. S., & Fox, J. M. (2021). Bioorthogonal chemistry. *Nature Reviews Methods Primers, 1*.

Selegard, R., Aronsson, C., Brommesson, C., Danmark, S., & Aili, D. (2017). Folding driven self-assembly of a stimuli-responsive peptide-hyaluronan hybrid hydrogel. *Scientific Reports, 7*(1), 7013.

Sternlicht, M. D., & Werb, Z. (2001). How matrix metalloproteinases regulate cell behavior. *Annual Review of Cell and Developmental Biology, 17*, 463–516.

Takahashi, A., Suzuki, Y., Suhara, T., Omichi, K., Shimizu, A., Hasegawa, K., … Ito, T. (2013). In situ cross-linkable hydrogel of hyaluronan produced via copper-free click chemistry. *Biomacromolecules, 14*(10), 3581–3588.

Tan, Y., Huang, H., Ayers, D. C., & Song, J. (2018). Modulating viscoelasticity, stiffness, and degradation of synthetic cellular niches via stoichiometric tuning of covalent versus dynamic noncovalent cross-linking. *ACS Central Science, 4*(8), 971–981.

Torres, A. L., Bidarra, S. J., Pinto, M. T., Aguiar, P. C., Silva, E. A., & Barrias, C. C. (2018). Guiding morphogenesis in cell-instructive microgels for therapeutic angiogenesis. *Biomaterials, 154*, 34–47.

Xu, M., Su, T., Jin, X., Li, Y., Yao, Y., Liu, K., … He, Y. (2022). Inflammation-mediated matrix remodeling of extracellular matrix-mimicking biomaterials in tissue engineering and regenerative medicine. *Acta Biomaterialia, 151*, 106–117.

Xue, M., & Jackson, C. J. (2015). Extracellular matrix reorganization during wound healing and its impact on abnormal scarring. *Advances in Wound Care (New Rochelle), 4*(3), 119–136.